

UC Berkeley

UC Berkeley Previously Published Works

Title

Natural Scene Statistics Account for the Representation of Scene Categories in Human Visual Cortex

Permalink

<https://escholarship.org/uc/item/32n0w537>

Journal

Neuron, 79(5)

ISSN

0896-6273

Authors

Stansbury, Dustin E
Naselaris, Thomas
Gallant, Jack L

Publication Date

2013-09-01

DOI

10.1016/j.neuron.2013.06.034

Peer reviewed



HHS Public Access

Author manuscript

Neuron. Author manuscript; available in PMC 2017 June 08.

Published in final edited form as:

Neuron. 2013 September 04; 79(5): 1025–1034. doi:10.1016/j.neuron.2013.06.034.

Natural scene statistics account for the representation of scene categories in human visual cortex

Dustin E. Stansbury¹, Thomas Naselaris^{2,†}, and Jack L. Gallant^{1,2,3}

¹Vision Science Group, University of California, Berkeley, CA 94720, USA

²Helen Wills Neuroscience Institute, University of California, Berkeley, CA 94720, USA

³Department of Psychology, University of California, Berkeley, CA 94720, USA

Abstract

During natural vision, humans categorize the scenes they encounter: an office, the beach, and so on. These categories are informed by knowledge of the way that objects co-occur in natural scenes. How does the human brain aggregate information about objects to represent scene categories? To explore this issue we used statistical learning methods to learn categories that objectively capture the co-occurrence statistics of objects in a large collection of natural scenes. Using the learned categories, we modeled fMRI brain signals evoked in human subjects when viewing images of scenes. We find that evoked activity across much of anterior visual cortex is explained by the learned categories. Furthermore, a decoder based on these scene categories accurately predicts the categories and objects comprising novel scenes from brain activity evoked by those scenes. These results suggest that the human brain represents scene categories that capture the co-occurrence statistics of objects in the world.

INTRODUCTION

During natural vision, humans categorize the scenes that they encounter. A scene category can often be inferred from the objects present in the scene. For example, a person can infer that she is at the beach by seeing water, sand, and sunbathers. Inferences can also be made in the opposite direction: the category “beach” is sufficient to elicit the recall of these objects plus many others such as towels, umbrellas, sandcastles, and so on. These objects are very different from those that would be recalled for another scene category such as an office. These observations suggest that humans use knowledge about how objects co-occur in the natural world to categorize natural scenes.

Correspondence should be addressed to: Jack L. Gallant, University of California at Berkeley, 3210 Tolman Hall #1650, Berkeley, CA 94720, gallant@berkeley.edu.

[†]Current address for Thomas Naselaris: Department of Neurosciences, Medical University of South Carolina, 173 Ashley Avenue, BSB 403, Charleston, SC 29425, USA

Conflict of Interest:

The authors declare no conflict of interest related to this work.

Publisher's Disclaimer: This is a PDF file of an unedited manuscript that has been accepted for publication. As a service to our customers we are providing this early version of the manuscript. The manuscript will undergo copyediting, typesetting, and review of the resulting proof before it is published in its final citable form. Please note that during the production process errors may be discovered which could affect the content, and all legal disclaimers that apply to the journal pertain.

There is substantial behavioral evidence to show that humans exploit the co-occurrence statistics of objects during natural vision. For example, object recognition is faster when objects in a scene are contextually consistent (Biederman, 1972; Biederman et al., 1973; Palmer, 1975). When a scene contains objects that are contextually inconsistent then scene categorization is more difficult (Davenport and Potter, 2004; Joubert et al., 2007). Despite the likely importance of object co-occurrence statistics for visual scene perception, few functional magnetic resonance imaging (fMRI) studies have investigated this issue systematically. Most previous fMRI studies have investigated isolated and decontextualized objects (Kanwisher et al., 1997; Downing et al., 2001), or a few, very broad scene categories (Epstein and Kanwisher, 1998; Peelen et al., 2009). However, two recent fMRI studies (Walther et al., 2009; MacEvoy and Epstein, 2011) provide some evidence that the human visual system represents information about individual objects during scene perception.

Here we test the hypothesis that the human visual system represents scene categories that capture the statistical relationships between objects in the natural world. To investigate this issue, we used a statistical learning algorithm originally developed to model large text corpora to learn scene categories that capture the co-occurrence statistics of objects found in a large collection of natural scenes. We then used fMRI to record blood-oxygenation-level-dependent (BOLD) activity evoked in the human brain when viewing natural scenes. Finally, we used the learned scene categories to model the tuning of individual voxels and we compared predictions of these models to alternative models based on object co-occurrence statistics that lack the statistical structure inherent in natural scenes.

We report three main results that are consistent with our hypothesis. First, much of anterior visual cortex represents scene categories that reflect the co-occurrence statistics of objects in natural scenes. Second, voxels located within and beyond the boundaries of many well-established functional ROIs in anterior visual cortex are tuned to mixtures of these scene categories. Third, scene categories and the specific objects that occur in novel scenes can be accurately decoded from evoked brain activity alone. Taken together, these results suggest that scene categories represented in the human brain capture the statistical relationships between objects in the natural world.

RESULTS

Learning Natural Scene Categories

To test whether the brain represents scene categories that reflect the co-occurrence statistics of objects in natural scenes, we first had to obtain such a set of categories. We used statistical learning methods to solve this problem (Figure 1A–B). First, we created a learning database by labeling the individual objects in a large collection of natural scenes (Figure 1A). The frequency counts of the objects that appeared in each scene in the learning database were then used as input to the Latent Dirichlet Allocation (LDA) learning algorithm (Blei et al., 2003). LDA was originally developed to learn underlying topics in a collection of documents based on the co-occurrence statistics of the words in the documents. When applied to the frequency counts of the objects in the learning database, the LDA algorithm learns an underlying set of scene categories that capture the co-occurrence statistics of the objects in the database.

LDA defines each scene category as a list of probabilities that are assigned to each of the object labels within an available vocabulary. Each probability reflects the likelihood that a specific object occurs in a scene that belongs to that category (Figure 1B). LDA learns the probabilities that define each scene category without supervision. However, the number of distinct categories the algorithm learns and the object label vocabulary must be specified by the experimenter. The vocabulary used for our study consisted of the most frequent objects in the learning database.

Figure 1B shows examples of scene categories learned by LDA from the learning database. Each of the learned categories can be named intuitively by inspecting the objects they are most likely to contain. For example, the first category in Figure 1B (left column) is aptly named “*Roadway*” because it is most likely to contain the objects “car,” “vehicle,” “highway,” “crash barrier,” and “street lamp.” The other examples shown in Figure 1B can also be assigned intuitive names that describe typical natural scenes. Once a set of scene categories has been learned, the LDA algorithm also offers a probabilistic inference procedure that can be used estimate the probability that a new scene belongs to each of the learned categories, conditioned on the objects in the new scene.

Voxel-wise Encoding Models Based on Learned Scene Categories

To determine whether the brain represents the scene categories learned by LDA we recorded BOLD brain activity evoked when human subjects viewed 1260 individual natural scene images. We used the LDA probabilistic inference procedure to estimate the probability that each of the presented stimulus scenes belonged to each of a learned set of categories. For instance, if a scene contained the objects “plate,” “table,” “fish,” and “beverage,” LDA would assign the scene a high probability of belonging to the “*Dining*” category in Figure 1B, a lower probability to the “*Aquatic*” category, and near zero probability to the remaining categories (Figure 1C, green oval).

The category probabilities inferred for each stimulus scene were used to construct voxel-wise encoding models. The encoding model for each voxel consisted of a set of weights that best mapped the inferred category probabilities of the stimulus scenes onto the BOLD responses evoked by the scenes (Figure 1C, green hexagon). Model weights were estimated using regularized linear regression applied independently for each subject and voxel. The prediction accuracy for each voxel-wise encoding model was defined to be the correlation coefficient (Pearson’s r score) between the responses evoked by a novel set of stimulus scenes and the responses to those scenes predicted by the model.

Introspection suggests that humans can conceive of a vast number of distinct objects and scene categories. However, because the spatial and temporal resolution of fMRI data are fairly coarse (Buxton, 2002), it is unlikely that all these objects or scene categories can be recovered from BOLD signals. BOLD signal-to-noise ratios (SNR) also vary dramatically across individuals, so the amount of information that can be recovered from individual fMRI data also varies. Therefore, before proceeding with further analysis of the voxel-wise models, we first identified the single set of scene categories that provided the best predictions of brain activity recorded from all subjects. To do so, we examined how the amount of accurately-predicted cortical territory across subjects varied with specific settings

of the number of individual scene categories and object vocabulary size assumed by the LDA algorithm during category learning. Specifically, we incremented the number of individual categories learned from 2 to 40 while also varying the size of the object label vocabulary from the 25 most frequent to 950 most frequent objects in the learning database (see Experimental Procedures for further details). Figure 2A shows the relative amount of accurately-predicted cortical territory across subjects based on each setting. Accurate predictions are stable across a wide range of settings.

Across subjects, the encoding models perform best when based on 20 individual categories and composed of a vocabulary 850 objects (Figure 2A, indicated by red dot; for individual subject results, see Supplemental Figure S3). Examples of these categories are displayed in Figure 2B (for an interpretation of all 20 categories, see Supplemental Figures S4–S5). Previous fMRI studies have only used 2–8 distinct categories and 2–200 individual objects (see Walther et al., 2009; MacEvoy and Epstein, 2011). Thus, our results show there is more information in BOLD signals related to encoding scene categories than has been previously appreciated.

We next tested whether natural scene categories were necessary to accurately model the measured fMRI data. We derived a set of null scene categories by training LDA on artificial scenes. The artificial scenes were created by scrambling the objects in the learning database across scenes, thus removing the natural statistical structure of object co-occurrences inherent in the original learning database. If the brain incorporates information about the co-occurrence statistics of objects in natural scenes, then the prediction accuracy of encoding models based upon these null scene categories should be much poorer than encoding models based on scene categories learned from natural scenes.

Indeed, we find that encoding models based on the categories learned from natural scenes provide significantly better predictions of brain activity than do encoding models based on the null categories, and for all subjects ($p < 1 \times 10^{-10}$ for all subjects, Wilcoxon rank-sum test for differences in median prediction accuracy across all cortical voxels and candidate scene category settings; subject S1: $W(15025164) = 9.96 \times 10^{13}$; subject S2: $W(24440399) = 3.04 \times 10^{14}$; subject S3: $W(15778360) = 9.93 \times 10^{13}$; subject S4: $W(14705625) = 1.09 \times 10^{14}$). In a set of supplemental analyses, we also compared the LDA-based models to several other plausible models of scene category representation. We find that the LDA-based models provide superior prediction accuracy to all these alternative models (see Supplemental Figures S12–S15). These results support our central hypothesis that the human brain encodes categories that reflect the co-occurrence statistics of objects in natural scenes.

Categories Learned From Natural Scenes Explain Selectivity in Many Anterior Visual ROIs

Previous fMRI studies have identified functional regions of interest (ROIs) tuned to very broad scene categories, such as places (Epstein and Kanwisher, 1998), as well as to narrow object categories such as faces (Kanwisher et al., 1997) or body parts (Downing et al., 2001). Can selectivity in these regions be explained in terms of the categories learned from natural scene object statistics?

We evaluated scene category tuning for voxels located within the boundaries of several conventional functional ROIs: the fusiform face area (FFA; Kanwisher et al., 1997), the occipital face area (OFA; Gauthier et al., 2000), the extrastriate body area (EBA; Downing et al., 2001), the parahippocampal place area (PPA; Epstein and Kanwisher, 1998), the transverse occipital sulcus (TOS; Nakamura et al., 2000; Grill-Spector, 2003; Hason et al., 2003), retrosplenial cortex (RSC; Maguire, 2001) and lateral occipital cortex (LO; Malach et al., 1995).

Figure 3A shows the boundaries of these ROIs, identified using separate functional localizer experiments, and projected on the cortical flat map of one representative subject. The color of each location on the cortical map indicates the prediction accuracy of the corresponding encoding model. All encoding models were based on the 20 best scene categories identified across subjects. These data show that the encoding models accurately predict responses of voxels located in many ROIs within anterior visual cortex. To quantify this effect, we calculated the proportion of response variance explained by the encoding models, averaged across all voxels within each ROI. We find that the average proportion of variance explained to be significantly greater than chance for every anterior visual cortex ROI, and for all subjects ($p < 0.01$; see Experimental Procedures for details). Thus, selectivity in many previously identified ROIs can be explained in terms of tuning to scene categories learned from natural scene statistics.

To determine whether scene category tuning is consistent with tuning reported in earlier localizer studies, we visualize the weights of encoding models fit to voxels within each ROI. Figure 3C shows encoding model weights averaged across all voxels located within each function ROI. Scene category selectivity is broadly consistent with the results of previous functional localizer experiments. For example, previous studies have suggested that PPA is selective for presence of buildings (Epstein and Kanwisher, 1998). The LDA algorithm suggests that images containing buildings are most likely to belong to the “*Urban/Street*” category (see Figure 2B), and we find that voxels within PPA have large weights for the “*Urban/Street*” category (see Supplemental Figures S4–S5). To take another example, previous studies have suggested that OFA is selective for the presence of human faces (Gauthier et al., 2000). Under the trained LDA model, images containing faces are most likely to belong to the “*Portrait*” category (see Supplemental Figures S4–S5), and we find that voxels within OFA have large weights for the “*Portrait*” category.

Although category tuning within functional ROIs is generally consistent with previous reports, Figure 3C demonstrates that tuning is clearly more complicated than assumed previously. In particular, many functional ROIs are tuned for more than one scene category. For example, both FFA and OFA are thought to be selective for human faces, but voxels in both these areas also have large weights for the “*Plants*” category. Additionally, area TOS, an ROI generally associated with encoding information important for navigation, has relatively large weights for the “*Portrait*” and “*People Moving*” categories. Thus, our results suggest that tuning in conventional ROIs may be more diverse than generally believed (for additional evidence, see Huth et al., 2012 and Naselaris et al., 2012).

Decoding Natural Scene Categories From Evoked Brain Activity

The results presented thus far suggest that information about natural scene categories is encoded in the activity of many voxels located in anterior visual cortex. It should therefore be possible to decode these scene categories from brain activity evoked by viewing a scene. To investigate this possibility, we constructed a decoder for each subject that uses voxel activity evoked in anterior visual cortex to predict the probability that a viewed scene belongs to each of 20 best scene categories identified across subjects. To maximize performance, the decoder used only those voxels for which the encoding models produced accurate predictions on a held-out portion of the model estimation data (for details, see Experimental Procedures).

We used the decoder to predict the 20 category probabilities for 126 novel scenes that had not been used to construct the decoder. Figure 4A shows several examples of the category probabilities predicted by the decoder. The scene in the upper right of Figure 4A depicts a harbor in front of a city skyline. The predicted category probabilities indicate that the scene is most likely a mixture of the categories “*Urban*” and “*Boatway*”, which is an accurate description of the scene. Inspection of the other examples in the Figure suggests that the predicted scene category probabilities accurately describe many different types of natural scenes.

To quantify the accuracy of each decoder, we calculated the correlation (Pearson’s r) between the scene category probabilities predicted by the decoder and the probabilities inferred using the LDA algorithm (conditioned on the labeled objects in each scene). Figure 4B shows the distribution of decoding accuracies across all decoded scenes, for each subject. The median accuracies and 95% confidence interval on median estimates are indicated by the black cross-hairs. Most of the novel scenes are decoded significantly for all subjects. Prediction accuracy across all scenes exhibited systematically greater-than-chance performance for all subjects ($p < 0.02$ for all subjects, Wilcoxon rank-sum test; subject S1: $W(126) = 18585$; subject S2: $W(126) = 17274$; subject S3: $W(126) = 17018$; subject S4: $W(126) = 19214$). The voxels selected for the decoding analysis summarized in Figure 4 were located throughout the visual cortex. However, we also find that accurate decoding can be obtained using the responses of subsets of voxels located within specific ROIs (see Supplemental Figures S16–S19).

Predicting the Objects that Occur in Decoded Natural Scenes

Our results suggest that the visual system represents scene categories that capture the co-occurrence statistics of objects in the natural world. This suggests that we should be able to predict accurately the likely objects in a scene based on the scene category probabilities decoded from evoked brain activity.

To investigate this issue, we estimated the probability that each of the 850 objects in the vocabulary for the single best set of scene categories identified across subjects occurred in each of the 126 decoded validation set scenes. The probabilities were estimated by combining the decoded category probabilities with the probabilistic relationship between categories and objects established by LDA learning algorithm during category learning (see

Experimental Procedures for details). The resulting probabilities give an estimate of the likelihood that each of the 850 objects occurs in each of the 126 decoded scenes.

In Figure 4A, labels in the black boxes indicate the most likely objects estimated for the corresponding decoded scene. For the harbor and skyline scene at upper right, the most probable objects predicted for the scene are “building,” “sky,” “tree,” “water,” “car,” “road,” and “boat.” All of these objects either occur in the scene or are consistent with the scene context. Inspection of the other examples in the Figure suggests that the most probable objects are generally consistent with the scene category.

To quantify how accurately the objects were decoded, we used the distribution of object probabilities estimated for each scene to calculate the likelihood of labeled objects in the scene. We then calculated the likelihood of the labeled objects from a naive distribution that assumes all 850 objects are equally likely to occur. The ratio of these likelihoods provides a measure of accuracy for the estimated object probabilities. Likelihood ratios greater than one indicate that the estimated object probabilities better predict the labeled objects in the scene than by picking objects at random (see Experimental Procedures for details).

Figure 4C shows the distribution of likelihood ratios for each subject, calculated for all 126 decoded scenes. The medians and 95% confidence intervals of the median estimates are indicated by the black cross-hairs. Object prediction accuracy across all scenes indicates systematically greater-than-chance performance for all subjects ($p < 1 \times 10^{-15}$ for all subjects, Wilcoxon rank-sum test; subject S1: $W(126) = 9983$; subject S2: $W(126) = 11375$; subject S3: $W(126) = 11103$; subject S4: $W(126) = 10715$).

The estimated object probabilities and the likelihood ratio analysis both show that the objects that are likely to occur in a scene can be predicted probabilistically from natural scene categories that are encoded in human brain activity. This suggests that humans might use a probabilistic strategy to help infer the likely objects in a scene from fragmentary information available at any point in time.

DISCUSSION

This study provides compelling evidence that the human visual system encodes scene categories that reflect the co-occurrence statistics of objects in the natural world. First, categories that capture co-occurrence statistics are consistent with our intuitive interpretations of natural scenes. Second, voxel-wise encoding models based on these categories accurately predict visually evoked BOLD activity across much of anterior visual cortex, including within several conventional functional ROIs. Finally, the category of a scene and its constituent objects can be decoded from BOLD activity evoked by viewing the scene.

Previous studies of scene representation in the human brain used subjective categories that were selected by the experimenters. In contrast, our study used a data-driven, statistical algorithm (LDA) to learn the intrinsic categorical structure of natural scenes from object labels. These learned, intrinsic scene categories provide a more objective foundation for scene perception research than is possible using subjective categories.

One previous study of scene perception used a similar statistical learning approach to investigate the intrinsic category structure of natural scenes (Fei-Fei and Perona, 2005). In that study the input to the learning algorithm was visual features of intermediate spatial complexity. Because our goal was to determine whether the brain represents the object co-occurrence statistics of natural scenes, we used object labels of natural scenes as input to the learning algorithm rather than intermediate visual features.

The voxel-wise modeling and decoding framework employed here (Kay et al., 2008; Mitchell et al., 2008; Naselaris et al., 2009; Naselaris et al., 2012; Nishimoto et al., 2011; Thirion et al., 2006) provides a powerful alternative to conventional methods based on statistical parametric mapping (Friston et al., 1996) or multivariate pattern analysis (MVPA; Norman et al., 2006). Studies based on statistical mapping or MVPA do not aim to produce explicit predictive models of voxel tuning, so it is difficult to generalize their results beyond the specific stimuli or task conditions used in each study. In contrast, the goal of voxel-wise modeling is to produce models that can accurately predict responses to arbitrary, novel stimuli or task conditions. A key strategy for developing theoretical models of natural systems has been to validate model predictions under novel conditions (Hastie et al., 2008). We believe that this strategy is also critically important for developing theories of representation in the human brain.

Our results generally corroborate the many previous reports of object selectivity in anterior visual cortex. However, we find that tuning properties in this part of visual cortex are more complex than reported in previous studies (see Supplemental Figures S7, S8–S11, and S16–S19 for supporting results). This difference likely reflects the sensitivity afforded by the voxel-wise modeling and decoding framework. Still, much work remains before we can claim a complete understanding of what and how information is represented in anterior visual cortex (Huth et al., 2012 and Naselaris et al., 2012).

Several recent studies (Kim and Biederman, 2011; MacEvoy and Epstein, 2011; Peelen et al., 2009) have suggested that the lateral occipital complex (LO) represents, in part, the identity of scene categories based on the objects therein. Taken together these studies suggest that some sub-regions within LO should be accurately predicted by models that link objects with scene categories. Our study employs one such model. We find that the encoding models based on natural scene categories provide accurate predictions of activity in anterior portions of LO (Figure 3A–B). Note however, that our results do not necessarily imply that LO represents scene categories explicitly (see Supplemental Figures 16–19 for further analyses).

Functional MRI provides only a coarse proxy of neural activity and has a low SNR. In order to correctly interpret the results of fMRI experiments it is important to quantify how much information can be recovered from these data. Here we addressed this problem by testing many candidate models in order to determine a single set of scene categories that can be recovered reliably from the BOLD activity measured across all of our subjects (Figure 2A). This test places a clear empirical limit on the number of scene categories and objects that can be recovered from our data. These numbers are larger than what has typically been assumed in previous fMRI studies of scene perception (Epstein and Kanwisher, 1998; Peelen

et al., 2009; Walther et al., 2009; MacEvoy and Epstein, 2011), but they are still far smaller than the likely representational capacity of the human visual system.

Theoreticians have argued that the simple statistical properties of natural scenes explain selectivity to low-level features in peripheral sensory areas (Olshausen and Field, 1996; Lewicki, 2001; Smith and Lewicki, 2006). Behavioral data suggest that low-level natural scene statistics also influence the perception of scene categories (Oliva and Torralba, 2001). Though several qualitative theories have been proposed that link the object statistics of natural scenes with human scene perception (Biederman, 1981; Palmer, 1975), none have provided an objective, quantitative framework to support this link. The current study provides such a framework. Our data-driven, model-based approach shows that scene categories encoded in the human brain can be derived from the co-occurrence statistics of objects in natural scenes. This further suggests that the brain exploits natural scene statistics at multiple levels of abstraction. If this is true, then natural scene statistics might be used as a principled means to develop quantitative models of representation throughout the visual hierarchy.

The work reported here could be extended in several ways. For example, although the spatial distribution of objects within a scene appears to influence the representation of the scene (Biederman et al., 1982; Green and Hummel, 2006; Kim and Biederman 2011), the modeling framework used here makes no assumptions about the spatial distribution of objects within scenes. More sophisticated models that incorporate spatial statistics or other mediating factors such as attention may provide further information about the representation of scenes and scene categories in the human brain.

EXPERIMENTAL PROCEDURES

Functional MRI Data Acquisition

All fMRI data were collected at the UC Berkeley Brain Imaging Center using a 3 Tesla Siemens Tim Trio MR scanner (Siemens, Germany). For subjects S1, S3, and S4, a gradient-echo echo planar imaging sequence, combined with a custom fat saturation RF pulse, was used for functional data collection. Twenty-five axial slices covered occipital, occipito-parietal, and occipito-temporal cortex. Each slice had a $234 \times 234 \text{ mm}^2$ field of view, 2.60 mm slice thickness, and 0.39 mm slice gap (matrix size = 104×104 ; TR = 2009.9 ms; TE = 35 ms; flip angle = 74° ; voxel size = $2.25 \times 2.25 \times 2.99 \text{ mm}^3$).

For subject S2 only, a gradient-echo echo planar imaging sequence, combined with a custom water-specific excitation (fat-shunting) RF pulse was used for functional data collection. In this case thirty-one axial slices covered the entire brain, and each slice had a $224 \times 224 \text{ mm}^2$ field of view, 3.50 mm slice thickness, and 0.63 mm slice gap (matrix size = 100×100 ; TR = 2004.5 ms; TE = 33 ms; flip angle = 74° ; voxel size = $2.24 \times 2.24 \times 4.13 \text{ mm}^3$).

Subject S1 experienced severe visual occlusion of the stimuli when the whole head coil was used. Therefore, for subject S1 the back portion (20 channels) of the Siemens 32 channel quadrature receive head coil was used as a surface coil. The full 32 channel head coil was used for subjects S2, S3 and S4.

Stimuli

All stimuli consisted of color images selected from a large database of natural scenes collected from various sources. Each image was presented on an isoluminant gray background and subtended the central $20^\circ \times 20^\circ$ square of the visual field. Images were presented in successive 4 second trials. On each trial a photo was shown for 1 second at 5 Hertz, followed by 3 second period where only the gray background was present. A central fixation square was superimposed at the center of the display, subtending $0.2^\circ \times 0.2^\circ$ of the visual field. To facilitate fixation, the fixation square was randomly permuted in color (red, green, blue, white) at a rate of 3 Hertz. No eye tracking was performed during stimulus presentation. However, all subjects in the study were highly trained psychophysical observers having extensive experience with fixation tasks, and preliminary data collected during an identical visual task showed that the subject cohort maintained stable fixation. Note also that the visual stimuli contained no object labels.

Experimental Design

Functional MRI experiments consisted of interleaved runs that contained images from separate model estimation and validation sets. Data were collected over six sessions for subjects S1 and S4, and seven sessions for subjects S2 and S3. Each of the 35 estimation set runs was 5.23 minutes in duration and consisted of 36 distinct images presented two times each. Evoked responses to these 1260 images were used during model estimation. Each of 21 5.23 minute-long validation set runs consisted of 6 distinct images presented 12 times each. The evoked responses to these 126 images were used during model validation. All images were randomly selected for each run with no repeated images across runs.

fMRI Data Processing

The SPM8 package (University College, London, UK) was used to perform motion correction, co-registration and reslicing of functional images. All other preprocessing of functional data was performed using custom software (MATLAB®, R2010a, MathWorks Inc. Natick, MA). Preprocessing was conducted across all sessions for each subject, using the first run of the first session as the reference. For each voxel, the preprocessed time series was used to estimate the hemodynamic response function (Kay et al, 2007). Deconvolving each voxel time course from the stimulus design matrix produced an estimate of the response amplitude—a single value—evoked by each image, for each voxel. These response amplitude values were used in both model estimation and validation stages of data analysis. Retinotopic visual cortex was identified in separate scan sessions using conventional methods (Hansen et al. 2007). Standard functional localizers (Spiridon et. al., 2006) were also collected in separate scan sessions and were used to identify the anatomical boundaries of conventional ROIs.

Learning Database and Stimulus Datasets

Natural scene categories were learned using Latent Dirichlet Allocation (Blei et al., 2003; Supplemental Figure S1 for more details). The LDA algorithm was applied to the object labels of a learning database of 4116 natural scenes compiled from two image datasets. The first image dataset (Lotus Hill; Yao et al., 2007) provided 2903 (71 percent) of the learning

database scenes. The remaining scenes were sampled from an image dataset that was created in house. In both datasets, all objects within the visible area of each image were outlined and labeled. Each in-house image was labeled by one of 15 naïve labelers. Since each image was labeled by a single labeler, no labels were combined when compiling the databases. In a supplemental analysis we verify that scene context created negligible bias in the statistics of the object labels (Supplemental Figure S2). Ambiguous labels, misspelled labels, and rare labels having synonyms within the learning database were edited accordingly (see Supplemental Procedures 1). Note that the 1260 stimulus scenes in the estimation set were sampled from the learning database. The validation set consisted of an independent set of 126 natural scenes labeled in house.

Voxel-wise Encoding Modeling Analysis

Encoding models were estimated separately for each voxel using 80 percent of the responses to the estimation set stimuli selected at random. The model weights were estimated using regularized linear regression in order to best map the scene category probabilities for a stimulus scene onto the voxel responses evoked when viewing that scene. The category probabilities for a stimulus scene were calculated from the posterior distribution of the LDA inference procedure, conditioned on the labeled objects in the scene (see Supplemental Procedure 6 for details). Half of the remaining 20 percent of the estimation data was used to determine model regularization parameters and the other half of the estimation data was used to estimate model prediction accuracy (see Supplemental Procedure 7 for more details on encoding model parameter estimation).

Prediction accuracy estimates were used to determine the single best set of categories across subjects. For each of 760 different scene category settings (defining the number of distinct categories and vocabulary size assumed by LDA during learning), we calculated the number of voxels with prediction accuracy above a statistical significance threshold (correlation coefficient > 0.21 ; $p < 0.01$; see Supplemental Procedure 8 for details on defining statistically significant prediction accuracy). This resulted in a vector of 760 values for each subject, where each entry in the vector provided an estimate of the amount of cortical territory that was accurately predicted by encoding models based on each category setting. To combine the cortical territory estimates across subjects, the vector for each subject was normalized to sum to one (normalization was done to control for differences in brain size and signal-to-noise ratios across subjects) and the Hadamard (element-wise) product of the normalized vectors was calculated. This resulted in a combined distribution of 760 values (see Figure 2A). The peak of the combined distribution gave the single best set of categories across subjects. For more details on this issue see Supplemental Procedure 9.

When calculating the proportion of response variance explained in each ROI by the encoding models, statistical significance was determined by permutation. Specifically, the proportion of variance explained was estimated using the responses to the validation set for each voxel-wise encoding model. These explained variance estimates were then permuted across all cortical locations and the average was estimated within each functional ROI. Thus, each permutation produced a random sample of average explained variance within the boundaries of each functional ROI. Statistical significance was defined as the upper 99th

percentile of the distribution of average explained variance estimates calculated within each ROI after 1000 voxel permutations. For more details on this procedure see Supplemental Procedure 10.

Decoding Analysis

Voxels were selected for the decoding analysis based on the predictive accuracy of their corresponding encoding models on the held-out estimation data set. To control for multiple comparisons during voxel selection, the predictive accuracy threshold was defined as a correlation coefficient greater than 0.34; $p < 5 \times 10^{-5}$, which is roughly the inverse of the number of cortical voxels in each subject. Using this criterion, 512 voxels were selected for subject S1, 158 for S2, 147 for S3, and 93 for S4.

Decoders were estimated using the selected voxels' responses to the scenes in the estimation set. Decoder weights were estimated using elastic-net-regularized multinomial regression (Friedman et al, 2008) using 80 percent of the estimation set data. The remaining 10 percent of the estimation responses were used to determine model regularization parameters. (The 10 percent of the estimation responses that were used to calculate encoding model prediction accuracies for voxel selection were not used to estimate the decoder). After weight estimation, the decoders were used to predict the probability that each scene in the validation set belonged to each of the 20 best scene categories identified across subjects from the responses evoked within the selected population of voxels. For more details on the decoding parameter estimation see Supplemental Procedure 13.

Decoder prediction accuracy for each scene was defined to be the correlation coefficient (Pearson's r) calculated between the category probabilities predicted by the decoder and the category probabilities inferred using LDA, and conditioned on the objects that were labeled in each scene. Statistical significance of decoder prediction accuracy across all scenes was determined using a Wilcoxon rank-sum test comparing the distribution of decoder prediction accuracies to a null distribution of prediction accuracies. For more details, see Supplemental Procedures 13.

Using the category probabilities predicted by the decoder for each scene in the validation set, we repeatedly picked from the 850 objects comprising the object vocabulary for the 20 best scene categories identified across subjects. Each object was picked by first drawing a category index with probability defined by the decoded scene category probabilities, followed by picking an object label with probability defined by the learned LDA model parameters. The learned LDA model parameters capture the statistical correlations of the objects in the learning database. Thus the frequency of an object being picked also obeyed this correlation. The frequency distribution resulting from 10,000 independent object label picks was then normalized. The result defined an estimated distribution of occurrence probabilities for the objects in the vocabulary. Statistical significance of object decoding accuracy across all scenes was determined using a Wilcoxon rank-sum test comparing the distribution of likelihood ratios for the decoder to a null distribution of likelihood ratios. For more details on this issue see Supplemental Procedures 14.

Supplementary Material

Refer to Web version on PubMed Central for supplementary material.

Acknowledgments

This work was supported by grants to JLG from the National Eye Institute (EY019684), the National Institute of Mental Health (MH66990) and the National Science Foundation Center for the Science of Information (CCF-0939370). We thank An Vu for data collection assistance, and Tom Griffiths, Shinji Nishimoto, Tolga Cukur, Mark Lescoarte, Michael Oliver, Alex Huth, James Gao, Natalia Bilenko, Anwar Nunez, Ben Dichter, and Melanie Miller for helpful discussions and comments.

References

- Biederman I. Perceiving real-world scenes. *Science*. 1972; 177(43):77–80. [PubMed: 5041781]
- Biederman I, Glass AL, Stacy W. Searching for objects in real-world scenes. *Journal of Experimental Psychology*. 1973; 97:22–27. [PubMed: 4704195]
- Biederman, I. On the semantics of a glance at a scene. In: Hlilsdale, M Kubovy, Pomerantz, JR., editors. *Perceptual Organization*. New Jersey: Lawrence Erlbaum; 1981. p. 213-263.
- Biederman I, Mezzanotte RJ, Rabinowitz JC. Scene perception: detecting and judging objects undergoing relational violations. *Cognitive Psychology*. 1982; 14:143–177. [PubMed: 7083801]
- Blei DM, Ng AY, Jordan MI. Latent Dirichlet Allocation. *Journal of Machine Learning Research*. 2003; 3(4–5):993–1022.
- Buxton, RB. *Introduction to Functional Magnetic Resonance Imaging Book Pack: Principles and Techniques*. Cambridge University Press; 2002.
- Davenport JL, Potter MC. Scene consistency in object and background perception. *Psychological Science*. 2004; 15(8):559–564. [PubMed: 15271002]
- Downing PE, Jiang Y, Shuman M, Kanwisher N. A Cortical Area Selective for Visual Processing of the Human Body. *Science*. 2001; 293(5539):2470–2473. [PubMed: 11577239]
- Epstein RA, Kanwisher N. A cortical representation of the local visual environment. *Nature*. 1998; 392(6676):598–601. [PubMed: 9560155]
- Evans, EF. *Handbook of Sensory Physiology*. Vol. 5. Berlin: Springer; 1975. Cochlear nerve and cochlear nucleus; p. 1-108.
- Fei-Fei, L., Perona, P. A Bayesian hierarchical model for learning natural scene categories. *IEEE Computer Society Conference on Computer Vision and Pattern Recognition*; 2005; 2005. p. 524-531.
- Gauthier I, Tarr MJ, Moylan J, Skudlarski P, Gore JC, Anderson AW. The fusiform “face area” is part of a network that processes faces at the individual level. *Journal of Cognitive Neuroscience*. 2000; 12(3):495–504. [PubMed: 10931774]
- Greene M, Oliva A. Recognition of natural scenes from global properties: Seeing the forest without representing the trees. *Cognitive Psychology*. 2009; 58:137–176. [PubMed: 18762289]
- Green CB, Hummel JE. Familiar interacting object pairs are perceptually grouped. *Journal of Experimental Psychology: Human Perception and Performance*. 2006; 32(5):1107–1119. [PubMed: 17002525]
- Grill-Spector K. The neural basis of object perception. *Current Opinion in Neurobiology*. 2003; 13(2): 159–166. [PubMed: 12744968]
- Fei-Fei, L., Perona, P. A Bayesian hierarchical model for learning natural scene categories. *IEEE Computer Society Conference on Computer Vision and Pattern Recognition*; 2005; 2005. p. 524-531.
- Friedman JH, Hastie T, Tibshirani R. Regularized Paths for Generalized Linear Models via Coordinate Descent. *Journal of Statistical Software*. 2008; 33(1)
- Friston KJ, Holmes A, Poline JB, Price CJ, Frith CD. Detecting Activations in PET and fMRI: Levels of Inference and Power. *NeuroImage*. 1996; 4(3):223–235. [PubMed: 9345513]

- Hansen KA, Kay KN, Gallant JL. Topographic Organization in and near Human Visual Area V4. *The Journal of Neuroscience*. 2007; 27(44):11896–11911. [PubMed: 17978030]
- Harding, S., Cooke, M., König, P. Auditory Gist Perception: An Alternative to Attentional Selection of Auditory Streams?. In: Paletta, L., Rome, E., editors. *Attention in Cognitive Systems: Theories and Systems from an Interdisciplinary Viewpoint*. Springer-Verlag; 2008. p. 399–416.
- Hasson U, Harel M, Levy I, Malach R. Large-scale mirror-symmetry organization of human occipito-temporal object areas. *Neuron*. 2003; 37(6):1027–1041. [PubMed: 12670430]
- Hastie, T., Tibshirani, R., Friedman, JH. *The elements of statistical learning: data mining, inference, and prediction*. 2. New York: Springer; 2008. *Model Assessment and Selection*; p. 219–260.
- Hayworth KJ, Biederman I. Neural evidence for intermediate representations in object recognition. *Vision Research*. 2006; 46(23):4024–4031. [PubMed: 16979693]
- Hollingworth A, Henderson JM. Does consistent scene context facilitate object perception? *Journal of Experimental Psychology. General*. 1998; 127(4):398–415. [PubMed: 9857494]
- Huth AG, Nishimoto S, Vu AT, Gallant JL. A continuous semantic space describes the representation of thousands of object and action categories across the human brain. *Neuron*. 2012; 76:1210–1224. [PubMed: 23259955]
- Jones JP, Palmer LA. The two-dimensional spatial structure of simple receptive fields in cat striate cortex. *Journal of Neurophysiology*. 1987; 58(6):1187–1211. [PubMed: 3437330]
- Joubert OR, Rousselet GA, Fize D, Fabre-Thorpe M. Processing scene context: fast categorization and object interference. *Vision Research*. 2007; 47(26):3286–3297. [PubMed: 17967472]
- Kanwisher N, McDermott J, Chun MM. The fusiform face area: a module in human extrastriate cortex specialized for face perception. *The Journal of Neuroscience: The Official Journal of the Society for Neuroscience*. 1997; 17(11):4302–4311. [PubMed: 9151747]
- Kay KN, David SV, Prenger RJ, Hansen KA, Gallant JL. Modeling low-frequency fluctuation and hemodynamic response timecourse in event-related fMRI. *Human Brain Mapping*. 2008; 29(2):142–156. [PubMed: 17394212]
- Kay KN, Naselaris T, Prenger RJ, Gallant JL. Identifying natural images from human brain activity. *Nature*. 2008; 452(7185):352–355. [PubMed: 18322462]
- Kim J, Biederman I. Where do objects become scenes? *Journal of Vision*. 2009; 9:779–779.
- Koch C, Ullman S. Shifts in selective visual attention: towards the underlying neural circuitry. *Human Neurobiology*. 1985; 4(4):219–227. [PubMed: 3836989]
- Lou, T., Xu, J. Visual saliency based on natural scene statistics. 2011 *Seventh International Conference on Natural Computation*; 2011. p. 982–986.
- MacEvoy SP, Epstein RA. Constructing scenes from objects in human occipitotemporal cortex. *Nature Neuroscience*. 2011; 14:1323–1329. [PubMed: 21892156]
- Maguire EA. The retrosplenial contribution to human navigation: a review of lesion and neuroimaging findings. *Scandinavian Journal of Psychology*. 2001; 42(3):225–238. [PubMed: 11501737]
- Malach R, Reppas JB, Benson RR, Kwong KK, Jiang H, Kennedy WA, Ledden PJ, Brady TJ, Rosen BR, Tootell RB. Object-related activity revealed by functional magnetic resonance imaging in human occipital cortex. *Proc Natl Acad Sci U S A*. 1995; 92:8135–8139. [PubMed: 7667258]
- Mitchell TM, Shinkareva SV, Carlson A, Chang KM, Malave VL, Mason RA, Just MA. Predicting Human Brain Activity Associated with the Meanings of Nouns. *Science*. 2008; 320(5880):1191–1195. [PubMed: 18511683]
- Nakamura K, Kawashima R, Sato N, Nakamura A, Sugiura M, Kato T, Hatano K, et al. Functional delineation of the human occipito-temporal areas related to face and scene processing. *Brain*. 2000; 123(9):1903–1912. [PubMed: 10960054]
- Naselaris T, Prenger RJ, Kay KN, Oliver M, Gallant JL. Bayesian Reconstruction of Natural Images from Human Brain Activity. *Neuron*. 2009; 63:902–915. [PubMed: 19778517]
- Naselaris T, Stansbury DE, Gallant JL. Cortical representation of animate and inanimate objects in complex natural scenes. *Journal of Physiology-Paris*. 2012; 106(5–6):239–249.
- Nishimoto S, Vu AT, Naselaris T, Benjamini Y, Yu B, Gallant JL. Reconstructing Visual Experiences from Brain Activity Evoked by Natural Movies. *Current Biology*. 2011; 21(19):1641–1646. [PubMed: 21945275]

- Norman KA, Polyn SM, Detre GJ, Haxby JV. Beyond mind-reading: multi-voxel pattern analysis of fMRI data. *Trends in Cognitive Sciences*. 2006; 10(9):424–430. [PubMed: 16899397]
- Oliva A, Torralba A. Modeling the Shape of the Scene : A Holistic Representation of the Spatial Envelope. *International Journal of Computer Vision*. 2001; 42(3):145–175.
- Oliva A, Torralba A. The role of context in object recognition. *Trends in Cognitive Sciences*. 2007; 11:520–527. [PubMed: 18024143]
- Olshausen BA, Field DJ. Emergence of simple-cell receptive field properties by learning a sparse code for natural images. *Nature*. 1996; 381(6583):607–609. [PubMed: 8637596]
- Palmer SE. The effects of contextual scenes on the identification of objects. *Memory and Cognition*. 1975; 3:519–526. [PubMed: 24203874]
- Peelen MV, Fei-Fei L, Kastner S. Neural mechanisms of rapid natural scene categorization in human visual cortex. *Nature*. 2009; 460(7251):94–97. [PubMed: 19506558]
- Potter MC. Meaning in visual search. *Science*. 1975; 187(4180):965–966. [PubMed: 1145183]
- Smith EC, Lewicki MS. Efficient auditory coding. *Nature*. 2006; 439(7079):978–982. [PubMed: 16495999]
- Spiridon M, Fischl B, Kanwisher N. Location and spatial profile of category-specific regions in human extrastriate cortex. *Human Brain Mapping*. 2006; 27(1):77–89. [PubMed: 15966002]
- Thirion B, Duchesnay E, Hubbard E, Dubois J, Poline J-B, LeBihan D, Dehaene S. Inverse retinotopy: Inferring the visual content of images from brain activation patterns. *NeuroImage*. 2006; 33(4):1104–1116. [PubMed: 17029988]
- Torralba A, Oliva A. Statistics of natural image categories. *Network: Computation in neural systems*. 2003; 14:391–412.
- Ullman S, Vidal-Naquet M, Sali E. Visual features of intermediate complexity and their use in classification. *Nature Neuroscience*. 2002; 5(7):682–687. [PubMed: 12055634]
- Walther DB, Caddigan E, Fei-Fei L, Beck DM. Natural Scene Categories Revealed in Distributed Patterns of Activity in the Human Brain. *The Journal of Neuroscience*. 2009; 29(34):10573–10581. [PubMed: 19710310]
- Yao, B., Yang, X., Zhu, SC. Introduction to a large-scale general purpose ground truth database: methodology, annotation tool and benchmarks. *Proceedings of the 6th International Conference on Energy Minimization Methods in Computer Vision and Pattern Recognition*; 2007. p. 169-183.

Highlights

- The brain represents scene categories that reflect co-occurrence statistics of objects in scenes
- These scene categories are represented in many anterior visual regions of interest
- Scene categories and individual objects can be decoded from measured brain activity
- fMRI signals contains more information about categories than previously appreciated

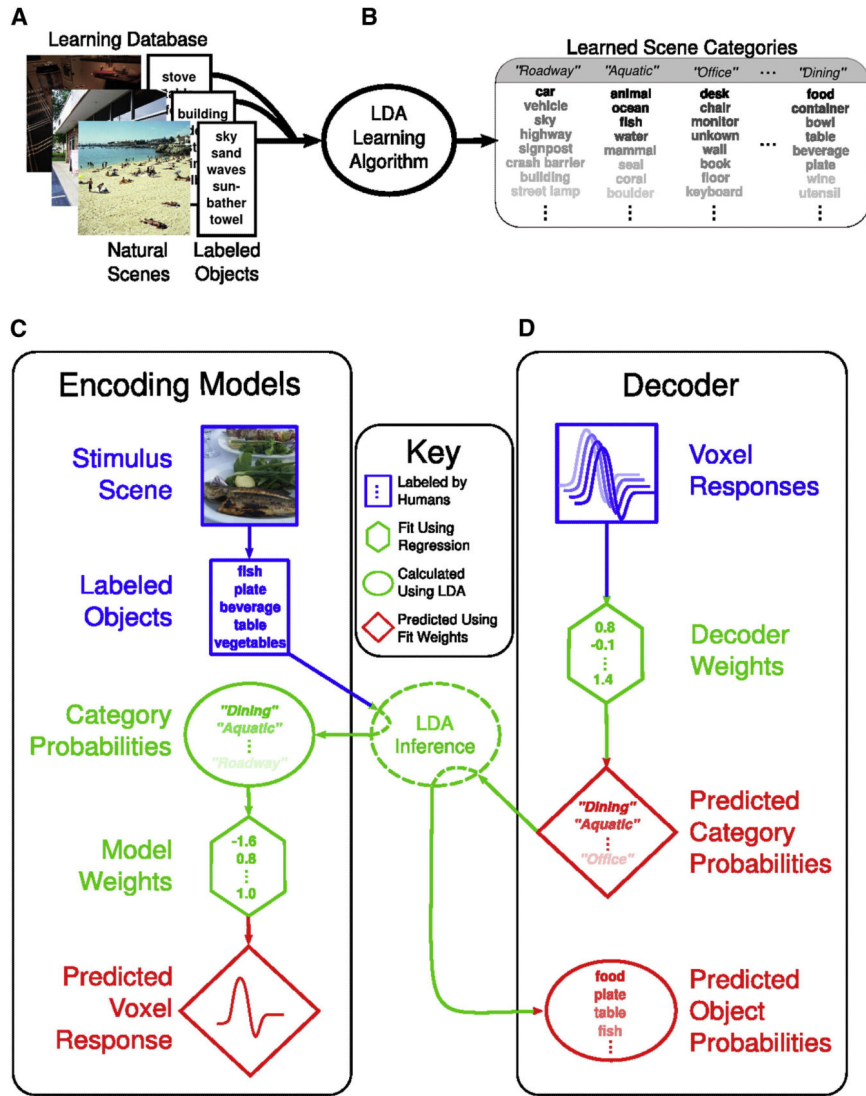


Figure 1. Overview of Analyses

(A) Learning Database. We compiled a large database of labeled natural scenes. All objects in each of the scenes were labeled by naïve participants. See also Supplemental Figure S2.

(B) Scene Categories Learned by LDA. LDA was used to learn scene categories that best capture the co-occurrence statistics of objects in the learning database. LDA defines each scene category as a list of probabilities, where each probability is the likelihood that any particular object within a fixed vocabulary will occur in a scene. Lists of probable objects for four example scene categories learned by LDA are shown on the right. Each list of object labels corresponds to a distinct scene category; within each list saturation indicates an object’s probability of occurrence. The experimenters, not the LDA algorithm, assigned intuitive category names in quotes. Once a set of categories is learned, LDA can also be used to infer the probability that a new scene belongs to each of the learned categories, conditioned on the objects in the new scene. See also Supplemental Figure S2.

(C) Voxel-wise Encoding Model Analysis. Voxel-wise encoding models were constructed to predict BOLD responses to stimulus scenes presented during an fMRI experiment. Blue

represents inputs to the encoding model, green represents intermediate model steps, and red represents model predictions. To generate predictions, the labels associated with each stimulus scene (blue box) are passed to the LDA algorithm (dashed green oval). LDA is used to infer from these labels the probability that the stimulus scene belongs to each of the learned categories (solid green oval). In this example the stimulus scene depicts a plate of fish so the scene categories “*Dining*” and “*Aquatic*” are highly probable (indicated by label saturation), while the category “*Roadway*” is much less probable. These probabilities are then transformed into a predicted BOLD response (red diamond) by a set of linear model weights (green hexagon). Model weights were fit independently for each voxel using a regularized linear regression procedure applied to the responses evoked by a set of training stimuli.

(D) Decoding Model Analysis. A decoder was constructed for each subject that uses BOLD signals evoked by a viewed stimulus scene to predict the probability that the scene belongs to each of a set of learned scene categories. Blue represents inputs to the decoder, green represents intermediate model steps, and red represents decoder predictions. To generate a set of category probability predictions for a scene (red diamond), evoked population voxel responses (blue box) are mapped onto the category probabilities by a set of multinomial model weights (green hexagon). Predicted scene category probabilities were then used in conjunction with the LDA algorithm to infer the probabilities that specific objects occurred in the viewed scene (red oval). The decoder weights were fit using regularized multinomial regression applied to the scene category probabilities inferred for a set of training stimuli using LDA and the responses to those stimuli.

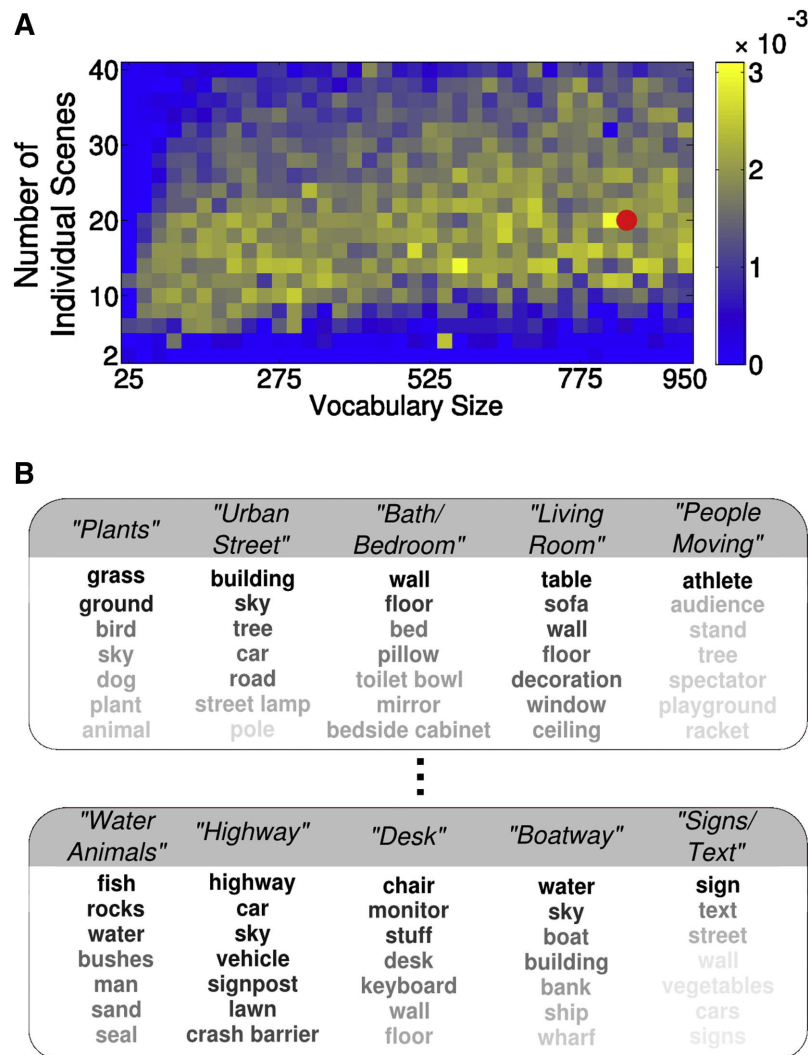


Figure 2. Identifying the Best Scene Categories for Modeling Data Across Subjects

(A) Encoding model performance across a range of settings for the specified number of distinct categories learned using LDA (y-axis) and vocabulary size (x-axis). Each pixel corresponds to one of the candidate scene categories learned by LDA when applied to the learning database. The color of each pixel represents the relative amount of cortical territory across subjects that is accurately predicted by encoding models based on a specific setting for the number of individual categories and vocabulary size. The number of individual categories was incremented from 2 to 40. The object vocabulary was varied from the 25 most frequent to the 950 most frequent objects in the learning database. The red dot identifies the number of individual categories and vocabulary size that produce accurate predictions for the largest amount of cortical territory across subjects. For individual results see Supplemental Figure S3.

(B) Ten examples taken from the 20 best scene categories identified across subjects (corresponding to the red dot in (A)). The seven most probable objects for each category are shown. Format is the same as in Figure 1B. See Supplemental Figures S4–S5 for interpretation of all 20 categories.

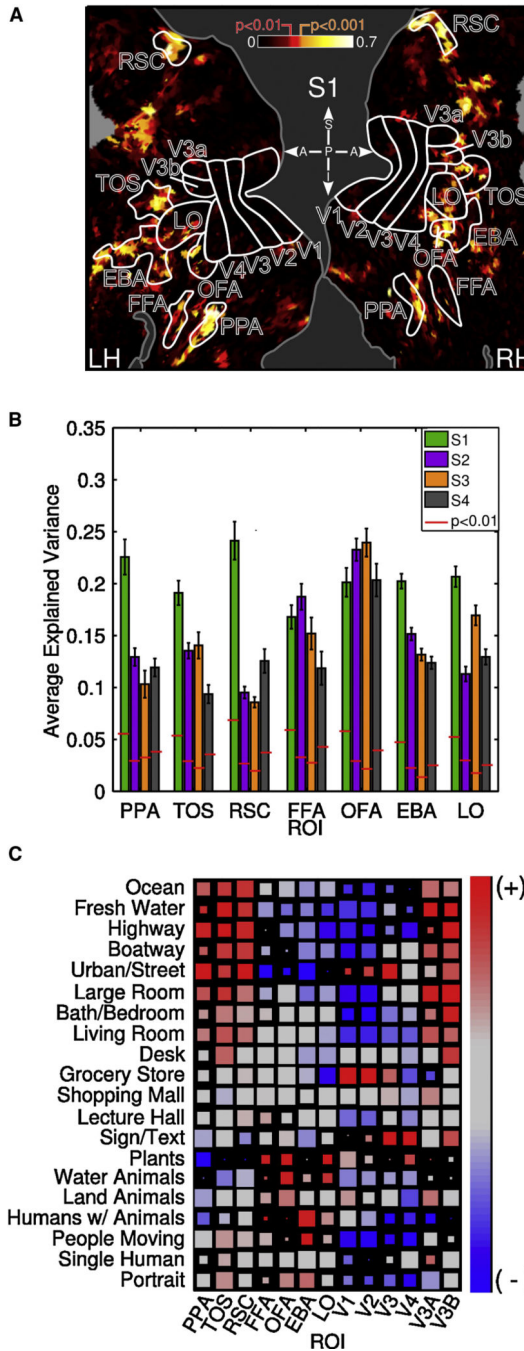


Figure 3. Scene Categories Learned from Natural Scenes are Encoded in Many Anterior Visual ROIs

(A) Encoding model prediction accuracies are mapped onto the left (LH) and right (RH) cortical surfaces of one representative subject (S1). Gray indicates areas outside of the scan boundary. Bright locations indicate voxels that are accurately predicted by the corresponding encoding model (prediction accuracy at two levels of statistical significance— $p < 0.01$ ($r = 0.21$) and $p < 0.001$ ($r = 0.28$)—are highlighted on the colorbar). ROIs identified in separate retinotopy and functional localizer experiments are outlined in white. The bright regions

overlap with a number of the ROIs in anterior visual cortex. These ROIs are associated with representing various high-level visual features. However, the activity of voxels in retinotopic visual areas (V1, V2, V3, V4, V3a, V3b) are not predicted accurately by the encoding models. Prediction accuracy was calculated on responses from a separate validation set of stimuli not used to estimate the model. ROI Abbreviations: Retinotopic Visual Areas 1–4 (V1–V4); Para-hippocampal Place Area (PPA); FFA, Fusiform Face Area (PPA); Extrastriate Body Area (EBA); Occipital Face Area (OFA); Retrosplenial Cortex (RSC); Transverse Occipital Sulcus (TOS). Center key: A=anterior; P=posterior, S=superior; I=inferior. For remaining subjects' data, see Supplemental Figure S6.

(B) Each bar indicates the average proportion of voxel response variance in an ROI that is explained by voxel-wise encoding models estimated for a single subject. Bar colors distinguish individual subjects. Error bars are standard error from the mean. For all anterior visual ROIs and for all subjects, encoding models based on scene categories learned from natural scenes explain a significant proportion of voxel response variance ($p < 0.01$, indicated by red lines).

(C) The average encoding model weights for voxels within distinct functional ROIs. Averages are calculated across all voxels located within the boundaries of an ROI, and across subjects. Each row displays the average weights for the scene category listed on the left margin. Each column distinguishes average weights for individual ROIs. The color of each pixel represents the positive (red) or negative (blue) average ROI weight for the corresponding category. The size of each pixel is inversely proportional to the magnitude of the standard error of the mean estimate; larger pixels indicate selectivity estimates with greater confidence. Standard error scaling is according to the data within an ROI (column). ROI tuning is generally consistent with previous findings. However, tuning also appears to be more complex than indicated by conventional ROI-based analyses For individual subjects' data, see Supplemental Figure S7; see also Supplemental Figures S8–S15.

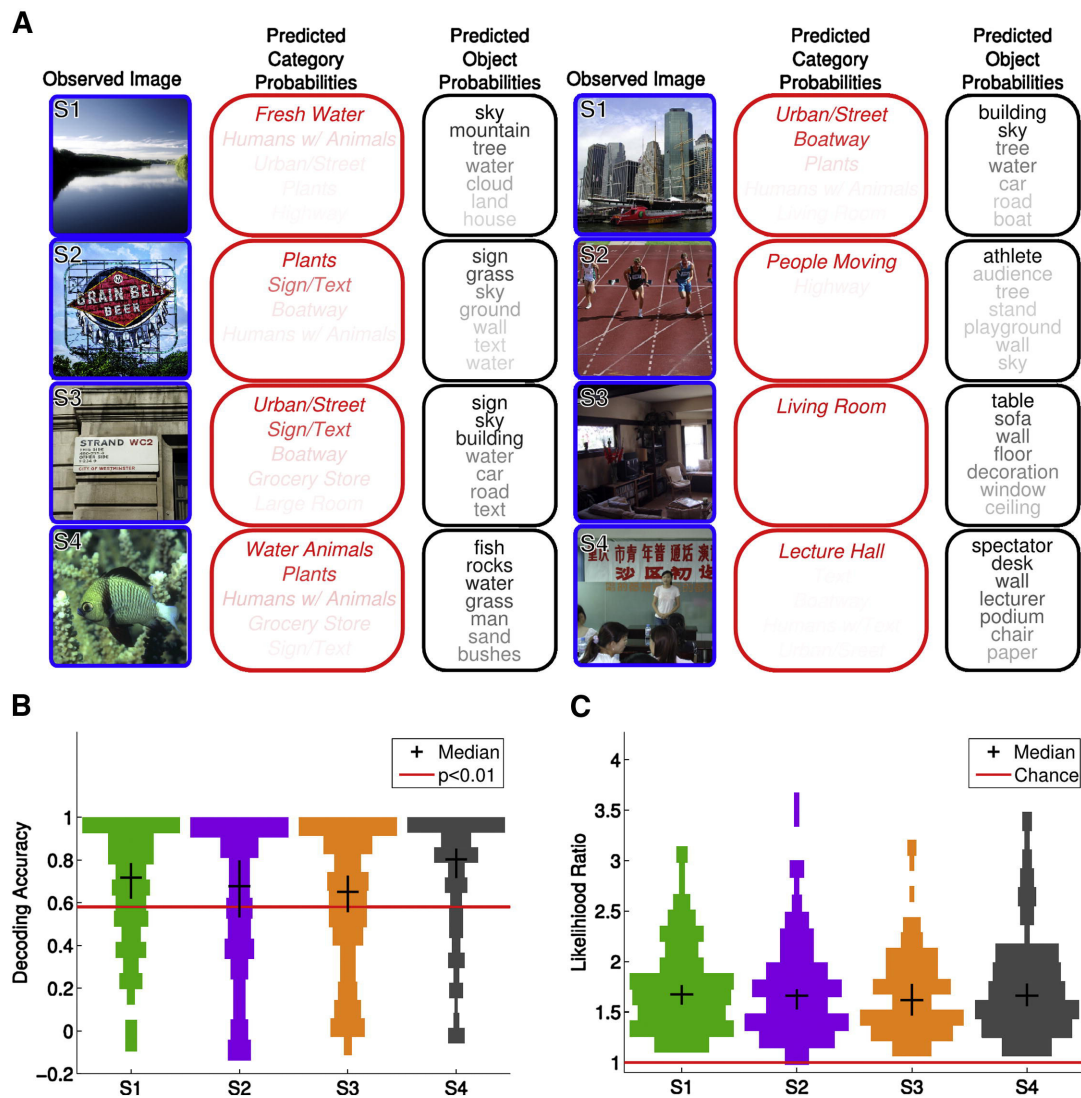


Figure 4. Scene Categories and Objects Decoded from Evoked BOLD Activity

(A) Examples of scene category and object probabilities decoded from evoked BOLD activity. Blue boxes (columns 1 and 4) display novel stimulus scenes observed by subjects S1 (top row) through S4 (bottom row). Each red box (columns 2 and 5) encloses the top category probabilities predicted by the decoder for the corresponding scene to the left. The saturation of each category name within the red boxes represents the predicted probability that the observed scene belongs to the corresponding category. Black boxes (columns 3 and 6) enclose the objects with the highest estimated probability of occurring in the observed scene to the left. The saturation of each label within the black boxes represents the estimated probability of the corresponding object occurring in the scene. See also Supplemental Figures S16–S19.

(B) Decoding accuracy for predicted category probabilities. Category decoding accuracy for a scene is the correlation coefficient between the category probabilities predicted by the decoder and the category probabilities inferred directly using LDA. Category probabilities were decoded for 126 novel scenes. Each plot shows the (horizontally mirrored) histogram

of decoding accuracies for a single subject. Median decoding accuracy and 95% confidence interval (CI) calculated across all decoded scenes is represented by black cross-hairs overlaid on each plot. For subjects S1–S4, median decoding accuracy was 0.72 (CI : [0.62, 0.78]), 0.68 (CI: [0.53, 0.80]), 0.65 (CI: [0.55, 0.72]), 0.80 (CI: [0.72, 0.85]), respectively. For a given image, decoding accuracy greater than 0.58 was considered statistically significant ($p < 0.01$), and is indicated by the red line. A large majority of the decoded scenes are statistically significant, including all examples shown in (A).

(C) Decoding accuracy for predicted object probabilities. Object decoding accuracy is the ratio of the likelihood of the objects labeled in each scene given the decoded category probabilities, to the likelihood of the labeled objects in each scene if all were selected with equal probability (chance). A likelihood ratio greater than one (red line) indicates that the objects in a scene are better predicted by the decoded object probabilities than by selecting objects randomly. Each plot shows the (horizontally mirrored) histogram of likelihood ratios for a single subject. Median likelihood ratios and 95% CI are represented by the black cross-hairs. For subjects S1–S4, the median likelihood ratio was 1.67 (CI: [1.57, 1.76]), 1.66 (CI: [1.52, 1.72]), 1.62 (CI: [1.45, 1.78]), 1.66 (CI: [1.56, 1.78]) for subjects S1–S4, respectively.